Morphological Instability in InAs/GaSb Superlattices due to Interfacial Bonds

J. H. Li,[1,2] D. W. Stokes,[1] O. Caha,[1] S. L. Ammu,[1,2,3] J. Bai,[4] K. E. Bassler,[1] and S. C. Moss[1,2]

[1]*Department of Physics, University of Houston, Houston, Texas 77204-5005, USA*

[2]*Texas Center for Superconductivity and Advanced Materials, University of Houston, Houston, Texas 77204-5002, USA*

[3]*Department of Electrical and Computer Engineering, University of Houston, Houston, Texas 77204-4007, USA*

[4]*Oak Ridge National Laboratory, Oak Ridge, Tennessee 37831, USA*

(Received 11 April 2005; published 26 August 2005)

Synchrotron x-ray diffraction is used to compare the misfit strain and composition in a self-organized nanowire array in an InAs/GaSb superlattice with InSb interfacial bonds to a planar InAs/GaSb superlattice with GaAs interfacial bonds. It is found that the morphological instability that occurs in the nanowire array results from the large misfit strain that the InSb interfacial bonds have in the nanowire array. Based on this result, we propose that tailoring the type of interfacial bonds during the epitaxial growth of III-V semiconductor films provides a novel approach for producing the technologically important morphological instability in anomalously thin layers.

DOI: 10.1103/PhysRevLett.95.096104 PACS numbers: 68.65.La, 61.10.Nz, 68.35.Dv, 68.65.Cd

The formation of self-organized semiconductor nanoscale structures (wells, wires, and dots), based on the morphological instability of strained molecular beam epitaxial (MBE) grown films, has been observed in many III-V systems and is of great importance from both a fundamental and technological point of view [1]. Although MBE growth is a nonequilibrium process that depends on kinetic parameters, the instability occurs when misfit strain energy can be reduced more than the surface energy will be increased if the morphology of the flat surface is perturbed [2,3]. Under these conditions a flat layer becomes unstable when its thickness reaches the critical layer thickness, at which the strain energy stored in the layer becomes large enough for it to be released via surface perturbation before dislocation formation. If the misfit between the size of the atoms of the growing layer and those of the substrate is small, then the critical layer thickness can be very large. This is the case for many III-V semiconductors, which have a misfit of less than 1% and critical layer thickness of hundreds of monolayers (ML) [4]. However, unusual instability phenomena have been observed in some noncommon anion strained III-V epitaxial single layers and heterostructures. For example, $In_{0.45}Ga_{0.55}As/InP(001)$ single layers with a misfit of 0.5% have instability at a very early stage of the growth [5]. Similarly, InAs/GaSb(001) heterostructures have a misfit of 0.62%, but unstable growth is observed at a thickness of a few ML [6]. In this Letter, we propose that these unusual instabilities in epitaxially grown InAs/GaSb(001) superlattices are due to the existence of certain interfacial (IF) chemical bonds between the layers that have a large misfit strain.

Using synchrotron x-ray diffraction and numerical modeling, we investigate the morphological instability in InAs/GaSb superlattices by comparing one with a modulated InAs nanowire structure grown on a GaSb(001) substrate with InSb IF bonds to a planar one without modulation grown on an InAs(001) substrate with GaAs IF bonds. In addition to having IF bonds that differ from those within the various layers, the InAs/GaSb systems can be complicated by anion incorporation [7,8]. We account for these complications and fit our data using calculations based on kinematical x-ray scattering theory that model the strain and composition within the layers. We find that the type of IF bond and the sign of the misfit in the InAs layers, which is altered by Sb incorporation, are crucial for the instability of the InAs layers and the spontaneous formation of the nanowires.

The samples studied were 140-period InAs/GaSb superlattices grown by solid-source MBE at 390 °C using As_4 and Sb_4. Each period contains 13 MLs of InAs, 13 MLs of GaSb, and a 1 ML IF layer, which was intentionally grown, using migration enhanced epitaxy (MEE) [6,9], to be InSb for the nanowire sample, and GaAs for the planar sample. The growth rate for all materials was 0.5 ML/s. X-ray diffraction measurements were carried out on a standard four-circle diffractometer at beamline X14A of the National Synchrotron Light Source (NSLS) at the Brookhaven National laboratory with an x-ray energy of 8.0 keV.

The morphologies of the samples were examined by cross-sectional scanning tunneling microscopy (XSTM), and the results have been reported elsewhere [9]. A reconstructed 3D structure of the nanowire sample, based on the XSTM measurements, is shown in Fig. 1. The thickness of the InAs layers (dark regions) undulates periodically along the $[\bar{1}10]$ direction. Moreover, the InAs regions are almost completely surrounded by the nearly uniform GaSb layers (bright regions). Along the perpendicular [110] directions, the thickness of the layers is uniform over a few to tens of microns. Thus, the InAs layers form a nanowire array. Since the nanowires at the neighboring InAs layers are out of phase, they have a face-centered rectangular (fcr) symmetry in the [110] cross section. The XSTM image of

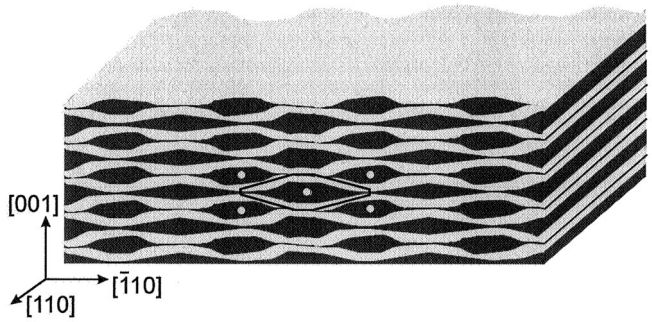

FIG. 1. A reconstructed 3D structure of the nanowire array in the nanowire sample [9]. Enclosed in the solid lines is the nanowire model used in our simulation. The bright circles mark a super fcr unit cell.

the planar sample, on the other hand, shows that the InAs and GaSb layers are flat indicating that the growth is stable.

To understand these observed morphologies, knowledge of the misfit strain of the superlattice is essential because strain is the driving force for the growth instability [2,3]. To determine the distribution of the misfit strain, we measured a reciprocal space map (RSM) around the ($\bar{2}$24) reciprocal lattice point of the average superlattice structure for the nanowire sample. The results are shown in Fig. 2(a). Both vertical and lateral high order satellite peaks are observed. The 2D satellite peaks, indexed by (m, n) (m and n denote the lateral and vertical order, respectively), also have a fcr symmetry in reciprocal space, which corresponds directly to that observed in real space. Note that the substrate peak is not clearly seen in this map due to large steps used in mapping. From the satellite spacing, we find that the average in- and out-of-plane periods of the nanowire array, Λ_x and Λ_z, are 1200 $\pm$ 50 Å and 160 $\pm$ 10 Å, respectively.

The diffracted x-ray intensity from a nanowire array can be calculated theoretically using kinematical x-ray scattering theory as

$$I(Q_x, Q_z) = \text{const} \times \left| F(Q_x, Q_z) \sum_m \sum_n \delta(Q_x - mG_x) \delta(Q_z - nG_z) \right|^2, \quad (1)$$

where Q_x and Q_z are projections of the scattering vector, $\mathbf{Q}$, in the $x \| [\bar{1}10]$ and $z \| [001]$ directions, respectively, $G_i = 2\pi/\Lambda_i$ ($i = x, z$), and (m, n) is the order of the 2D satellites. $F(Q_x, Q_z)$ is the structure factor of the super fcr unit cell [10]:

$$F(Q_x, Q_z) = (1 + e^{i(Q_x \Lambda_x/2 + Q_z \Lambda_z/2)}) \times \int \sigma(\mathbf{r}) \rho_w(\mathbf{r}) e^{i\mathbf{Q}\cdot[\mathbf{r}+\mathbf{u}(\mathbf{r})]} d\mathbf{r}, \quad (2)$$

where $\sigma(\mathbf{r})$ and $\rho_w(\mathbf{r})$ are the shape and electron density functions of a single nanowire, and $\mathbf{u}(\mathbf{r})$ is the displacement field. The shape function $\sigma(\mathbf{r})$ assumes the periodic

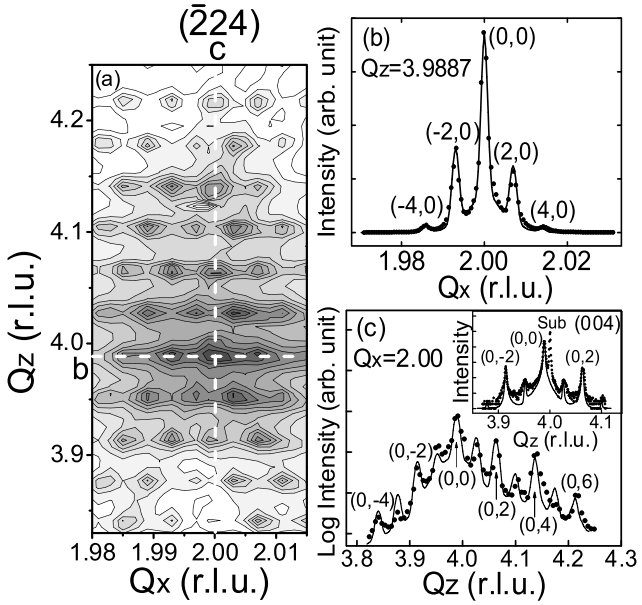

FIG. 2. (a) X-ray reciprocal space map around the ($\bar{2}$24) reciprocal lattice points of the nanowire sample. The logarithmic contour step is 0.235. (b) Q_x scan at $Q_z = 3.9887$. (c) Q_z scan at $Q_x = 2.00$. The inset in (c) is a (004) Q_z scan at $Q_x = 0$. Dots—experimental data; lines—simulation.

structure enclosed by the lines in Fig. 1, consisting of a hexagonal shaped InAs wire (dark area) surrounded by GaSb spacers (bright areas). The basic building block of the nanowire array is the super fcr unit cell marked by bright circles in Fig. 1. The electron density function $\rho_w(\mathbf{r})$ depends on $\sigma(\mathbf{r})$ and describes the composition of the layers, including any segregation or contamination. The displacement field, $\mathbf{u}(\mathbf{r})$, depends on $\sigma(\mathbf{r})$ and the composition. It is related to the misfit strain fields ε_{xx} and ε_{zz} along the lateral and vertical directions, respectively, by

$$\varepsilon_{xx} = \frac{\partial u_x}{\partial x} = \frac{a_x - a_{\text{sub}}}{a_{\text{sub}}}, \qquad \varepsilon_{zz} = \frac{\partial u_z}{\partial z} = \frac{a_z - a_{\text{sub}}}{a_{\text{sub}}}, \quad (3)$$

where a_x and a_z are the in- and out-of-plane lattice constants of the strained film, and a_{sub} is the lattice constant of the substrate. The calculated misfit fields, shown in Fig. 3, were determined by a direct solution of the equations of linear continuum elasticity using a boundary integral (BI) method that is an extension of the method used in Ref. [11]. Similar methods have proven to be valid for layers as thin as one monolayer [12]. It should be noted that these numerical solutions are highly nontrivial. In our case, a coupled set of BIs, one for each of the interfaces of the periodic structure, had to be calculated. Details of the numerical calculations will be presented elsewhere.

Using Eq. (1), we are able to model all essential features of the experimental RSM (note that peak width is dominated by the instrumental resolution). The dots in Fig. 2(b) show the intensity profile along Q_x at $Q_z = 3.9887$ that was extracted from the RSM. Because of the fcr symmetry,

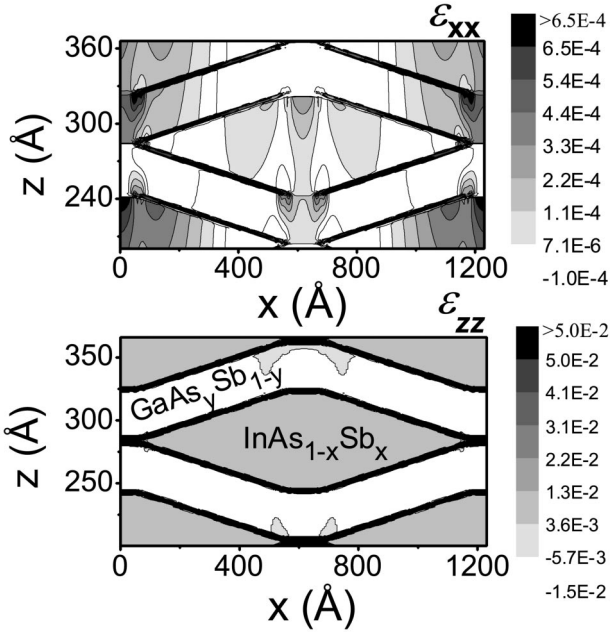

FIG. 3. In-plane and out-of-plane misfit strain ε_{xx} and ε_{zz}. Notice that the variation of strain in both the wire and spacer is very small and the strain is mostly concentrated at the interfaces.

only the even-order peaks can be seen in this profile. The most noticeable feature is that the satellite intensity is asymmetric about the zeroth order peak. To fit this feature, the average in-plane lattice constant, $a_{\parallel}$, in the InAs layers ($a_{\mathrm{InAs}} = 6.0584$ Å) and the interfacial InSb layers ($a_{\mathrm{InSb}} = 6.4789$ Å) must be assumed to be larger than that of GaSb ($a_{\mathrm{GaSb}} = 6.0961$ Å). The best fit, shown as a line in Fig. 2(b), was obtained by taking an average in-plane lattice constant of 6.1005 Å for both the "InAs" (whose actual composition is discussed below) and the InSb layers.

The distortion in the nanowire structure is also reflected in the out-of-plane lattice constant. To measure it, a Q_z scan around the GaSb(004) reciprocal lattice point was performed. The result is shown in the inset of Fig. 2(c). Here the GaSb substrate peak is resolved and is used as a reference for the determination of the out-of-plane lattice constant of the superlattice layers. The zeroth order satellite peak, located at $Q_z = 3.9887$, yields an average out-of-plane lattice constant of 6.1134 Å for the superlattice. This value is larger than 6.0882 Å, which is the value expected from the bulk values of the lattice and elastic constants for pure InAs, GaSb, and InSb, assuming 100% InSb interfacial bonds.

To account for these results, either InAs, GaSb, or both must have an increased out-of-plane lattice constant. This is possible if segregation and/or contamination of the group V atoms has occurred. Such contamination has previously been observed in this system [6–9,13,14], where Sb incorporation into InAs leads to an $InAs_{1-x}Sb_x$ alloy whose lattice constant increases with the Sb concentration; similarly, As incorporation in the GaSb leads to a $GaAs_ySb_{1-y}$ alloy whose lattice constant decreases with increase in the As concentration. Cross incorporation of group III atoms, Ga and In, is negligible as indicated by the XSTM experiments on this system [6,9,13]. As for the interfacial bonds, experiments have shown that the MEE growth technique is able to maintain over 95% of the desired interfacial bonds [15], and their effect on the average out-of-plane lattice constant is minor. The measured average out-of-plane lattice constant is thus a function of the alloy compositions.

To determine the alloy compositions, the (004) and ($\bar{2}24$) Q_z spectra were fit. The best fit is shown by the line in Fig. 2(c). That fit assumes Sb segregation and/or contamination of the InAs resulting in a $InAs_{0.88}Sb_{0.12}$ alloy and an As contamination of the GaSb resulting in a $GaAs_{0.05}Sb_{0.95}$ alloy that have an average out-of-plane lattice constant of 6.1180 Å and 6.0539 Å, respectively. As shown in Fig. 3, the continuum elasticity calculation reveals that ε_{zz} is almost uniform in the $InAs_{0.88}Sb_{0.12}$ and $GaAs_{0.05}Sb_{0.95}$ layers as well as at the interfaces. However, the magnitude of the misfit strain at the interface is an order of magnitude higher than that in the bulk film. Also, ε_{xx} fluctuates in a small range of about 5×10^{-4}, but overall ε_{xx} in the $InAs_{0.88}Sb_{0.12}$ layer is positive, indicating that the layer is slightly relaxed.

The average freestanding lattice constant, a_0, of the layer is obtained using Vegard's law from the alloy composition. The misfit, f, is calculated as $f = (a_0 - a_{\mathrm{sub}})/a_{\mathrm{sub}}$. The most important result is that the InAs nanowires, which were expected to have a negative misfit with respect to the substrate, have a positive misfit (+0.21%), and the "GaSb" spacers, which were expected to have zero misfit, have a negative misfit (−0.36%). Below, it will be discussed how the sign and magnitude of the misfit strain are important in the self-assembling of the nanowires.

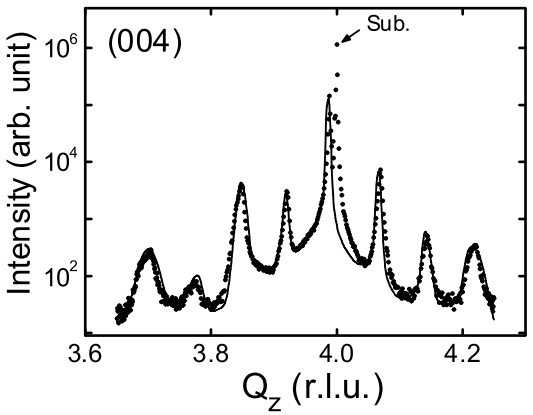

FIG. 4. X-ray (004) Q_z scan taken from the planar sample. Dots and line represent experimental data and calculation, respectively. The increase in peak width with order was fit using the Hendricks-Teller approach [19].

We now turn to the planar sample. Recall that it was grown on the InAs(001) substrate with GaAs IF bonds. Because the layers are flat, we have only taken a Q_z scan around the InAs(004) reciprocal lattice point. The result is shown in Fig. 4. To fit this profile, a structural model consisting of alternating $InAs_{1-x}Sb_x$ and $GaAs_ySb_{1-y}$ layers separated by GaAs interfacial bonds was considered. The best fit (line) to the data (dots) was obtained with $InAs_{0.88}Sb_{0.12}$ and $GaAs_{0.09}Sb_{0.91}$ alloys, which yields a misfit of $+0.83\%$ and -0.04%, respectively. Note that the Sb fraction in InAs is the same for both samples. The use of InAs, instead of GaSb, as the substrate for the planar sample, however, results in an increased misfit in the InAs(Sb) layers.

In comparing the nanowire and planar samples, we see that the $InAs_{0.88}Sb_{0.12}$ layers in the two samples both have positive misfits with respect to their substrate. However, the $InAs_{0.88}Sb_{0.12}$ layers in the nanowire sample with a smaller misfit of $+0.21\%$ are unstable, whereas the same layers in the planar sample with a larger misfit of $+0.83\%$ are stable. The only difference between the $InAs_{0.88}Sb_{0.12}$ layers in the two samples is that they were grown with different IF bonds, which have opposite misfits with respect to the substrates. The InSb IF bonds in the nanowire sample have a large positive misfit of $+6.28\%$ with respect to the substrate, which is an order of magnitude larger than that of the $InAs_{0.88}Sb_{0.12}$ layer, $+0.21\%$. In the planar sample, the GaAs bonds experience a large negative misfit of -6.69%, which is opposite to the sign of the misfit in the $InAs_{0.88}Sb_{0.12}$ layers, $+0.83\%$. This suggests that both the magnitude and sign of the misfit of the IF layer is key to the morphological instability of the $InAs_{0.88}Sb_{0.12}$ layers.

In the case of the nanowire sample, the $InAs_{0.88}Sb_{0.12}$ and the IF InSb both have a positive misfit. Thus, it is favorable for them to relax together. Since the strain energy is proportional to the layer thickness, the high misfit strain in the interfacial InSb substantially reduces the critical layer thickness of $InAs_{0.88}Sb_{0.12}$ making it possible for the onset of instability in just a few MLs [6,9]. In the case of the planar sample, the $InAs_{0.88}Sb_{0.12}$ and the interfacial GaAs have opposite misfits. The relaxation of these two materials involves atomic displacements in opposite directions; therefore, it is unfavorable for them to relax together, and, instead, they prevent each other from relaxing. Such a strain balancing mechanism has been used in the growth of strain-balanced superlattices [16]. This explains why stable growth of $InAs_{0.88}Sb_{0.12}$ was retained in the planar sample.

It is worth noting that although our experiments were performed on multilayer structures, the same effect can also cause modulation in thin single-layer films. For example, our model may be used to explain the result of Okada *et al.* [5] who showed that the growth of $In_xGa_{1-x}As$ single-layer film on InP(001) substrates is stable if the film has a positive misfit of 0.5% ($x = 0.605$) with respect to the substrate, but unstable if the film experiences a -0.5% misfit ($x = 0.45$). Because the IF bonds in this system are dominantly GaP [17], which upon formation over the InP substrate, experience a misfit strain up to -7.12%, the stable and unstable growth of the films with positive and negative misfits is thus expected.

In conclusion, we find that if the misfit of the IF layer is of the same sign as that of the overgrown layer, morphological instability can be triggered shortly after the beginning of growth. However, if the IF layer and the over layer experience an opposite misfit, they are stabilized. Our findings indicate that with proper design of the interfacial bonding, self-assembled nanostructures can be grown in material systems with a small misfit, which would otherwise be impossible. This explains the occurrence of the morphological instabilities observed in the epitaxially grown InAs/GaSb superlattice system, which has a variety of potential applications as lasers and detectors operating in the mid- to far-infrared region (3–30 μm) [18]. Therefore, our results demonstrate an approach that may be useful for creating a novel class of technologically important semiconductor nanostructures.

The authors are grateful to B. Z. Nosho, B. R. Bennett, and L. J. Whitman for supplying the samples. The work is supported by the NSF through Grants No. DMR-0237811 (D. W. S.), No. DMR-0406323 (K. E. B.), and No. DMR-0408539 (S. C. M.), by the Texas Center for Superconductivity and Advanced Materials, and by the Alfred P. Sloan Foundation.

[1] M. Law, J. Goldberger, and P. Yang, Annu. Rev. Mater. Res. **34**, 83 (2004).
[2] B. J. Spencer, P. W. Voorhees, and J. Tersoff, Phys. Rev. B **64**, 235318 (2001), and references there in.
[3] R. J. Asaro and W. A. Tiller, Metall. Trans. **3**, 1789 (1972); M. A. Grinfeld, Sov. Phys. Dokl. **31**, 831 (1986).
[4] Ch. Heyn, Phys. Rev. B **64**, 165306 (2001).
[5] T. Okada, G. C. Weatherly, and D. W. McComb, J. Appl. Phys. **81**, 2185 (1997).
[6] B. Z. Nosho *et al.*, J. Vac. Sci. Technol. B **19**, 1626 (2001).
[7] J. Steinshnider *et al.*, Phys. Rev. Lett. **85**, 4562 (2000).
[8] D. H. Chow *et al.*, J. Vac. Sci. Technol. B **8**, 710 (1990).
[9] B. Z. Nosho *et al.*, Appl. Phys. Lett. **81**, 4452 (2002).
[10] Q. Shen *et al.*, Phys. Rev. B **48**, 17967 (1993).
[11] W. H. Yang and D. J. Srolovitz, J. Mech. Phys. Solids **42**, 1551 (1994).
[12] T.-L. Lee *et al.*, Phys. Rev. B **60**, 13612 (1999).
[13] J. Harper *et al.*, Appl. Phys. Lett. **73**, 2805 (1998).
[14] D. W. Stokes *et al.*, J. Appl. Phys. **93**, 311 (2003).
[15] B. R. Bennett *et al.*, Appl. Phys. Lett. **63**, 949 (1993).
[16] For example, T. H. Chiu *et al.*, Appl. Phys. Lett. **62**, 340 (1993).
[17] P. E. Smith *et al.*, J. Vac. Sci. Technol. **22**, 554 (2004).
[18] Y. Wei *et al.*, Appl. Phys. Lett. **81**, 3675 (2002).
[19] S. Hendricks and E. J. Teller, J. Chem. Phys. **10**, 147 (1942).